IEEE Open Journal of
Power Electronics

Received 23 December 2025; revised 23 January 2026; accepted 4 February 2026. Date of publication 9 February 2026; date of current version 19 February 2026. The review of this article was arranged by Associate Editor Marco Jung.

Digital Object Identifier 10.1109/OJPEL.2026.3663079

Design Trade-Offs and Selection Guidelines for Isolated and Nonisolated Converters for In-Motion-Charging Buses

RUDOLF F. P. PATERNOST [1,2] (Member, IEEE), RICCARDO MANDRIOLI [3] (Senior Member, IEEE), IBRAHIM DIAB [4] (Member, IEEE), MIKOLAJ BARTŁOMIEJCZYK [5] (Member, IEEE), MATTIA RICCO [3] (Senior Member, IEEE), AND TÁRCIO A. S. BARROS [1] (Member, IEEE)

[1]Faculdade de Engenharia Elétrica e de Computação, Universidade Estadual de Campinas (UNICAMP), Campinas 13083-852, Brazil
[2]Av. Albert Einstein, 400 - Cidade Universitária, Campinas-SP 13083-852, Brazil
[3]Department of Electrical, Electronic and Information Engineering, University of Bologna, 40136 Bologna, Italy
[4]Electrical Sustainable Energy Department, Delft University of Technology (TU Delft), 2628 CD Delft, The Netherlands
[5]Department of Electrical Engineering for Transport, Gdańsk University of Technology, 80-233 Gdańsk, Poland

CORRESPONDING AUTHOR: RUDOLF F. P. PATERNOST (e-mail: rudolf2@unicamp.br)

This work was supported by Programa de Pesquisador de Pos-Doutorado (PPPD) at the Universidade Estadual de Campinas (UNICAMP).

ABSTRACT The increase in electrified transport has elevated the role of electric buses (e-buses) in addressing urban mobility challenges. Among the types of e-buses, there is the in-motion-charging (IMC) trolleybus, which is powered by DC overhead contact lines and has an on-board battery for traction outside overhead lines. A key challenge for IMC buses is the selection of the optimal on-board-charger (OBC) topology for charging their batteries. Ideally, the chosen OBC should have low weight and volume, in addition to operating with high efficiency levels. Additionally, there is a growing need for isolated DC-DC converter topologies to enhance safety and reduce the risk of electric shocks. However, the isolated topologies tend to have higher volume and weight and reduced efficiency due to the need for a high-frequency transformer (HFT). In this context, this article aims to provide design trade-offs and guidelines for choosing between isolated and non-isolated topologies for OBC in IMC trolleybuses, based on an analysis of their efficiency, weight, volume, and cost. A non-isolated interleaved buck-boost (IBB) and an isolated dual-active-bridge (DAB) converters are taken as the study-case. Results indicate strong potential for the IBB at switching frequencies above 75 kHz, primarily due to a significant reduction in the weight and volume of the magnetic components, with the weight of IBB being about 0.84 times that of the DAB at 100 kHz switching frequency. For lower frequencies, the DAB converter presents advantages in terms of magnetic compactness. The efficiency of both topologies remains at similar levels, with a slight advantage for the non-isolated one, achieving an average efficiency of up to 99.07%.

INDEX TERMS Electric buses, trolleybuses, on-board-chargers, dual-active-bridge, interleaved buck-boost, dual-phase-shift.

I. INTRODUCTION

The means of transport are responsible for a significant portion of overall energy consumption and pollutant gas emissions due to the prevalence of internal combustion engine vehicles in the world fleet. In this context, government institutions have proposed legislation and projects to reduce greenhouse gas (GHG) emissions. In the European Union, The European Green Deal initiative aims to cut transport pollution emissions by at least 55% and 90% by 2030 and 2050, respectively [1], [2]. In South America, Brazil has a program named Programa de Mobilidade Verde (MOVER) [3], that aims to encourage less polluting solutions in the transportation sector, involving vehicle electrification, advanced biofuels, energy efficiency, and other technologies, through incentives

for research and innovation. The electrification of mobility in metropolitan areas is a key measure to reduce GHG emissions in the transportation sector. Investments in electric buses (e-buses) offer a viable response to the increased demand for mobility while simultaneously reducing pollutant emissions in large and medium-sized cities.

Different types of e-buses can be classified based on their power source and mode of operation, and an e-bus type that is growing popular, mainly in medium-sized European cities and is also present in South American cities like São Paulo [4], is the trolleybuses. They are powered by a DC electrical infrastructure called catenary or overhead contact lines (OCL), with similar characteristics to some light railway modes, like tramways and subways. Trolleybuses can also be classified into two categories. The first one can be called conventional trolleybuses, with just an electrical drive and no storage system inside, always operating connected to the OCL. The second one is a type of trolleybus called in-motion-charging (IMC). Being a hybrid between a conventional trolleybus and a full battery-electric bus, the IMC system requires the OCL to recharge the battery while moving through the electrified stretch of the route. In the remaining part, where there is no contact line, the vehicle runs on battery [5], [6]. Several studies in the literature are considering IMC vehicles as the future generation of public transportation, including proposals for electrification projects using this technology [7], [8]. Although with different power levels, such considerations are also valid for tramways and e-bus systems charged at the depot.

A. ON-BOARD CHARGERS AND VEHICLE ISOLATION

In the IMC system, power electronics converters charge the battery pack using on-board-chargers (OBC). Unlike rail vehicles, catenary-powered buses and trucks are isolated from the ground by rubber tires, posing a systemic risk to passengers: a simple isolation failure in the chassis can cause an electric shock. This risk cannot be addressed by grounding the vehicle using the negative pole of the catenary, because this process is unreliable [9]. Therefore, to enhance safety, technical compliances regarding galvanic isolation of electrically propelled road vehicles (ISO 6469-3:2021 [10], EN 61140:2016 [11]), and charging of DC systems applicable to electric buses (EN 61851-23:2014 [12]) generally require a second level of isolation (i.e. double isolation).

The mentioned double isolation is fulfilled by the manufacturers in mainly two different forms. In the first one, physical isolators separate the battery pack and the converter from the chassis of the vehicle, while a non-isolated topology is used as OBC (Fig. 1(a)). In the second form, an isolated topology is used as OBC, in which a high-frequency-transformer (HFT) isolates the battery pack from the DC link, ensuring the second-level isolation (Fig. 1(b)). These two scenarios result in different values of weight, volume, cost, and efficiency for the OBC used in IMC trolleybus.

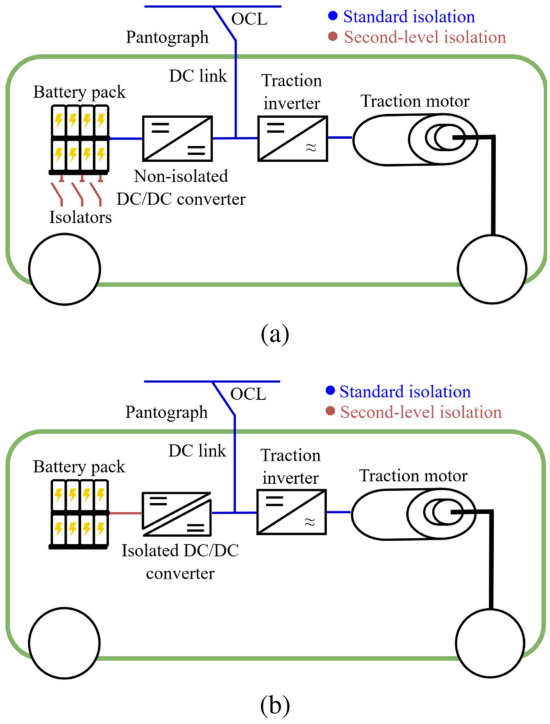

FIGURE 1. Types of isolation in trolleybuses. (a) Second-level isolation is performed by physical isolators. (b) Second-level isolation is performed by an isolated OBC topology.

B. STATE OF THE ART

The scientific literature contains studies that provide an overview of charging strategies for e-buses, along with reviews of OBC topologies typically employed for each strategy. As an example, the paper on [13] presents a comprehensive bibliometric analysis and comparison of e-bus charging strategies, including depot charging, en-route (or opportunity) charging, and in-motion charging. It covers aspects like power flow capabilities, costs, grid impacts, and efficiency. However, the work does not address power electronic converter topologies used to charge e-buses. While [14] presents a comprehensive review of on-board and off-board chargers for EVs, it does not specifically address the topologies used or their applicability to e-buses. For a more technical exploration of converters used for e-bus, [15] provides an overview of isolated DC-DC converter topologies used for medium voltage e-bus fast charging, with a particular focus on dual active bridge (DAB) converters and their application across various power levels. However, no cost evaluation or comparison is included in the study. A comparison between isolated and non-isolated converter topologies is made in [16], but with a particular focus on e-buses charging at the depot.

Going into more detail about OBC topologies, some prototypes were already developed, with the DAB converter emerging as a promising and feasible solution for such applications, as indicated by studies in the literature [9], [17], [18], [19], [20]. Additionally, DAB can also be designed for

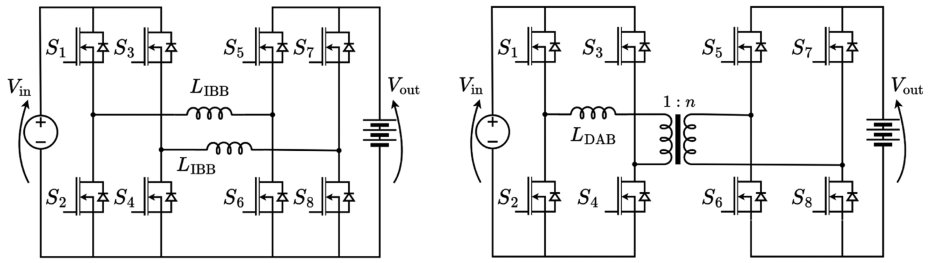

(a) Two-phase interleaved buck-boost converter (b) Dual-active-bridge converter

FIGURE 2. Converters under consideration for actuation as OBC in IMC trolleybuses. V_{in} and V_{out} indicate input and output voltages, respectively.

multiport converters [21]. This topology can meet the voltage and power demands required by catenary systems that power trolleybuses or e-trucks, which, depending on the system, can vary between 500 V and 1000 V, with a nominal voltage of 750 V, or between 400 V and 800 V, with a nominal voltage of 600 V, according to [22], [23]. This corresponds to a variation of 33% in comparison to their nominal voltages. Consequently, the converter design must comply with the aforementioned voltage ranges to meet the requirements of different OCL systems. Furthermore, OBCs for IMC vehicles need to handle power levels up to 500 kW [24], or even higher in the case of e-trucks. While bidirectional power flow is beneficial, allowing energy to be injected back into the OCL when voltage levels approach the lower limit, is not a strict requirement. The studies [9], [18], [19] explored DAB converters specifically designed for the mentioned requirements.

The various OBC topology options, arising from the different types of double isolation used in IMC trolleybuses, lead to variations in the converters' performance, physical characteristics, and economic parameters. In this context, there is a particular need for a comparative analysis between isolated and non-isolated converters for IMC applications. With structural similarities to the DAB, the interleaved buck-boost (IBB) converter emerges as an appropriate choice for a comparative analysis between isolated and non-isolated topologies adapted to IMC applications. Both have bidirectional capabilities and can be constructed with two full bridges or four identical half-bridges, resulting in comparable symmetry and the same additional circuitry, such as drivers, sensors, and auxiliaries. This would lead to a comparable cost of semiconductor devices and size of magnetic components. While isolated topologies offer safety benefits, the economic and performance trade-offs, especially in terms of efficiency, cost, and volume, remain unclear compared to non-isolated alternatives.

C. PAPERS CONTRIBUTIONS

This article aims to address the mentioned gaps by providing design trade-offs and selection guidelines based on an analysis of the efficiency, weight, volume, and cost of an IBB (Fig. 2(a)) and a DAB (Fig. 2(b)) converters used as OBC for IMC trolleybus applications. Although these topologies are well-established in the literature, a comparative evaluation under unified design conditions, such as input and output voltage range, output power levels, different switching frequencies, and selected semiconductors, is lacking. By combining accurate modeling and component-level cost/volume breakdowns, this study provides a quantitative and reproducible basis for topology selection considering the possibilities of vehicle isolation architectures in IMC trolleybuses' OBC systems, filling the gap between academic studies and industry needs.

II. DESIGN APPROACH USED FOR THE CONVERTERS AND MAGNETIC DEVICES

This section presents the generic design procedure for the converters IBB, which is designed to operate in continuous conduction mode, and DAB, as well as the design procedure for the magnetic devices and conductors.

A. INTERLEAVED BUCK-BOOST CONVERTER DESIGN APPROACH

The required inductance value for each phase of the IBB, based on the peak-to-peak current ripple at the battery side (ΔI_{batt}), can be calculated using the following equations, for the boost and buck operation, respectively:

$$L_{IBB}^{boost} = \frac{pV_{in}D_{eq}}{Nf_{Sw}\Delta I_{batt}}, \tag{1}$$

$$L_{IBB}^{buck} = \frac{V_{in}(1-D_{eq})D_{eq}}{Nf_{Sw}\Delta I_{batt}}, \tag{2}$$

where V_{in} is the converter's input voltage, f_{Sw} is the switching frequency, N is the number of phases in parallel, p is the ceiling of the product between N and the duty cycle of the converter (D), calculated based on:

$$D = \begin{cases} \frac{V_{out}}{V_{in}}, & \text{if } V_{in} > V_{out} \\ 1 - \frac{V_{in}}{V_{out}}, & \text{if } V_{in} \leq V_{out} \end{cases}, \tag{3}$$

where V_{out} is the converter's output voltage, and D_{eq} is the equivalent duty-cycle of the IBB, given by:

$$D_{eq} = N\left(D - \frac{p-1}{N}\right). \tag{4}$$

Once the theoretical inductance values for each phase are calculated, it is necessary to design the inductors taking into

account the constructive aspect based on different core types, which present different cross-sectional areas A_c, lengths l_c, and core geometry. The actual inductance L_{ind} is calculated according to the material of the core, number of turns N, and air gap, considering two U-core assembled to form a closed magnetic path:

$$L_{ind} = \frac{N^2}{\mathcal{R}} = \frac{N^2 \mu_0 A_c}{\frac{l_c - 2l_g}{\mu_r} + 2l_g}, \tag{5}$$

where l_g is the air gap length, μ_r is the core's relative permeability, μ_0 is the permeability of free space, and $\mathcal{R}$ is the total reluctance of the inductor.

The magnetic flux density [25] is calculated and used to evaluate the core losses of the inductor:

$$B_{ind}^{max} = \frac{L_{ind}}{NA_c}\left(I_{avg|ind} + \frac{\Delta I}{2}\right), \tag{6}$$

where ΔI is the peak-to-peak ripple, and $I_{avg|ind}$ is the average inductor current.

B. DUAL-ACTIVE-BRIDGE CONVERTER DESIGN APPROACH

The required power designed for the application (P_{des}) is used to calculate the inductance of the DAB converter according to the equation below, applied when single-phase-shift (SPS) modulation is considered:

$$L_{DAB} = \frac{kV_{in}V_{out}}{f_{Sw}P_{des}}\phi(1-2\phi), \tag{7}$$

where k is the transformer ratio, and ϕ is the phase shift, $\phi \in [0; 0.25]$.

The DAB converter's real inductance is given considering an auxiliary inductor designed following the principles of (5), and the leakage inductance of the HFT, estimated by:

$$L_{HFT} = l_{\delta 1} + l'_{\delta 2} = \frac{N_1^2}{R_T} - kM + k^2\left(\frac{N_2^2}{R_T} - \frac{M}{k}\right), \tag{8}$$

where $l_{\delta 1}$ is the leakage inductance of the primary, $l'_{\delta 2}$ is the leakage inductance of the secondary reflected to the primary, N_1 and N_2 are the number of windings in the primary and secondary, and M is the mutual inductance, given by:

$$M = k_c\sqrt{L_{11}L_{22}}, \tag{9}$$

where k_c is the HFT coupling factor, $L_{11} = \frac{N_1^2}{R_T}$, and $L_{22} = \frac{N_2^2}{R_T}$ are the self-inductance of the HFT primary and secondary, respectively. The total reluctance of the magnetic circuit is defined as:

$$R_T = \frac{1}{\mu_0 A_c}\left(\frac{l_c - 2l_g}{\mu_r} + 2l_g\right). \tag{10}$$

The expression for the magnetizing current is given by [26]:

$$I_m = \frac{V_{in}}{4f_{Sw}L_{11}}. \tag{11}$$

The paper [27] describes a strategy for computing magnetic induction, used to estimate HFT core loss. The peak value of magnetic induction is calculated by ignoring voltage drop on transistors, assuming a rectangular shape of the voltage waveforms, and taking $l_{\delta 1} = l'_{\delta 2}$.

$$B_{HFT}^{max} = \frac{V_1 T_s(1-\phi)}{2N_1 A_c^{HFT}}, \tag{12}$$

where V_1 is the voltage at the HFT primary side, T_s is the switching period, A_c^{HFT} is the HFT cross-sectional area.

This work considers the DAB operating with dual-phase-shift (DPS) modulation at low power levels, which occurs when the outer phase shift, ϕ_2 ($\phi_2 \in [0, 0.25]$), is below a certain threshold. In this case, the inner phase shift, ϕ_1 ($\phi_1 \in [0, 0.5]$), is calculated using (13), derived from the transmission power in DPS operation presented in [28]:

$$\phi_1 = \begin{cases} \sqrt{\phi_2(1-2\phi_2) - P \cdot \frac{f_{Sw}L_{DAB}}{kV_{in}V_{out}}}, & \text{if } \phi_1 \le \phi_2 \\ \frac{1}{2}(1 - \phi_2 - \frac{P}{\phi_2} \cdot \frac{f_{Sw}L_{DAB}}{kV_{in}V_{out}}), & \text{if } \phi_1 > \phi_2 \end{cases}, \tag{13}$$

where P is the power handled by the DAB converter.

C. PARALLEL OPERATION OF CONVERTER MODULES

Heavy-duty applications generally demand power levels that cannot be achieved with a single converter module. As a result, multiple modules must operate in parallel to satisfy the required power level. Accordingly, the procedure adopted in this paper is based on single-module characterization and phase-shedding theory [29], [30], [31]. Specifically, the converter is first simulated and optimized as a single module, obtaining its efficiency map over the operating range. The system-level efficiency for multiple modules in parallel is then extrapolated analytically by applying the phase-shedding principle. Namely, the efficiency η_N of a converter with N modules at the power P can be approximated by the efficiency of the single module η_1 as:

$$\eta_N(P) = \eta_1\left(\frac{P}{N}\right). \tag{14}$$

Then, the global efficiency is taken as the upper envelope of the N efficiency traces.

III. ON-BOARD-CHARGER COST EVALUATION METHOD

In the literature, the challenge of estimating OBC costs is often addressed by considering the number of active switches, magnetic components, and capacitors. Then, the cost of OBCs, C_{OBC}, can be evaluated based on the cost of each switch (C_{Sw}), magnetic devices (C_{mag}) and capacitors (C_{cap}) [32]:

$$C_{OBC} = C_{Sw}N_{Sw} + C_{mag}N_{mag} + C_{cap}N_{cap}. \tag{15}$$

where parameters N_{Sw}, N_{mag}, N_{cap} are the number of power switches, magnetic devices, and capacitors, respectively.

In general, OBCs are composed by converter units with a certain topology, in which the units function in coordination. Supposing that the installed power of one unit is defined as $P_{inst|unit}$, and the number of switches of one unit

TABLE 1. IBB and DAB Converters Module Main Parameters

Parameter	Value
Nominal power	50 kW [33]
Input voltage range	380 V – 1000 V [33]
Maximum input current	87.5 A [33]
Output voltage range	500 V – 850 V [33]
Maximum output current	77.5 A [33]
HFT turn ratio (DAB)	1

is $N_{Sw|unit}$, incrementing the installed power (P_{inst}) of the OBC requires introducing entire converter units, therefore the cost will increase in "steps" rather than smoothly. In other words, for each increase in power within a $P_{inst|unit}$ range (e.g., 1 kW to $P_{inst|unit}$, $P_{inst|unit} + 1$ kW to $2 \cdot P_{inst|unit}$, etc.), the cost remains constant, as it does not require additional units. At each multiple of $P_{inst|unit}$ (e.g., $P_{inst|unit}$, $2 \cdot P_{inst|unit}$, $3 \cdot P_{inst|unit}$, etc.), the cost jumps up as a new converter unit is added. Therefore, the OBC's cost in function of the installed power, $C_{OBC}(P_{inst})$, can be described as:

$$C_{OBC}(P_{inst}) = \frac{P_{inst}}{P_{inst|unit}} C_{OBC|unit}, \tag{16}$$

where $C_{OBC|unit}$ is the cost of one unit.

IV. CASE STUDY DEFINITION

The case study in question is summarized in this section, including the power and voltage needs of both converters under examination, as well as the design specifications of the converters, magnetic cores, and cables. The DC catenary infrastructure of trolleybus systems typically operates at one of two voltage ranges: 400–800 V or 500–1000 V [22], depending on the voltage level adopted by the transportation company. Therefore, based on [33], the converters considered in this manuscript are designed to operate with an input voltage in the range between 380–1000 V, and the output voltage, at the battery side, operates in the range between 500–850 V (Table 1). In addition, the converters are designed to operate with a maximum continuous power of 200 kW, therefore, 4 modules of 50 kW each are considered to operate in coordination to reach the designed maximum output power.

A. SEMICONDUCTOR DEVICES AND SIMULATION TOOLS

The voltage and current requirements must be satisfied by semiconductor devices for the application under consideration. According to the specifications in [33], the maximum continuous current at the input and output of each 50 kW module are 85.5 A and 77.5 A, respectively (Table 1). Therefore, for simplification purposes, semiconductor devices with a voltage rating of at least 1200 V and a current rating of at least 100 A are considered for the IBB converter. For the DAB one, simulations showed that the semiconductor devices have to support a current of around 180 A in the most conservative situation. Therefore, the considered MOSFETS for the DAB converter have a rated current of at least 200 A. To meet these requirements, this work considers the SiC-MOSFET device SCT015W120G3-4AG [34] for the IBB converter, and the SiC-MOSFET device CAB004M12GM4 [35] for the DAB one. The conduction losses of the semiconductor devices used for the IBB converter were modeled using the drain-current (I_D) vs drain-source-voltage (V_{DS}) characteristics, considering gate-source voltage (V_{GS}) of 18 V, as recommended by the manufacturer [34]. The switching-loss model is based on the switching energy characteristics as a function of I_D. For the DAB converter, conduction losses of the semiconductor devices were modeled using the I_D–V_{DS} characteristics considering $V_{GS} = 15$ V, as recommended by the manufacturer [35]. The switching losses were modeled using the switching energy vs drain current characteristics. The mentioned curves were used as inputs to the simulation model in the PLECS 4.9 (Plexim GmbH) software [36], which was employed to obtain the converter's efficiency results. Auxiliary losses for both converters were modeled as the sum of gate driver losses and other system-level auxiliary losses. The gate driver losses (P_{gd}) can be calculated on a per-switch basis according to $P_{gd} = V_{GS} Q_q f_{Sw}$ [29], where Q_g is the gate charge, found in datasheets. In addition, a constant auxiliary loss of 20 W was assumed to account for the power consumption of the digital control electronics, voltage and current sensing circuits, auxiliary power supplies, and cooling fans. The auxiliary losses and gate driver losses are considered independent of the output power. All simulations were performed assuming a fixed junction temperature at 125°C to represent a worst-case operating condition, under which semiconductor losses are intentionally overestimated. This ensures that the comparative analysis remains generic and does not depend on the specific thermal design adopted in a given implementation.

B. SEMICONDUCTORS COST ESTIMATION

Manufacturers often provide SiC MOSFETs in different configurations, including discrete MOSFETs, half-bridges (two MOSFETs connected in series with a shared output point), and full-bridge modules (four MOSFETs arranged in a bridge-like structure). A survey conducted in different manufacturer's websites reveals that half-bridge modules are commonly available than full-bridge modules. While discrete devices cost less compared to modules, the latter are often equipped with measurement and protection structures, making them more expensive, but requiring minimal external circuitry.

To meet the operating requirements of the OBC, this work considers SiC MOSFETS devices with drain-to-source voltage rating of 1200 V and a continuous drain current ranging from 50 A to 400 A. As the application requires a current of 100 A for the IBB converter and 200 A for the DAB, specifically for devices rated between 50 A – 99 A, a parallel operation is assumed to meet the required current per topology. Consequently, the number of devices to implement the OBC increases proportionally to the current rating of the selected MOSFETs.

To evaluate the costs of OBCs, a survey was conducted based on the prices found in the marketplace of half-bridge, full-bridge, and discrete devices produced by the following

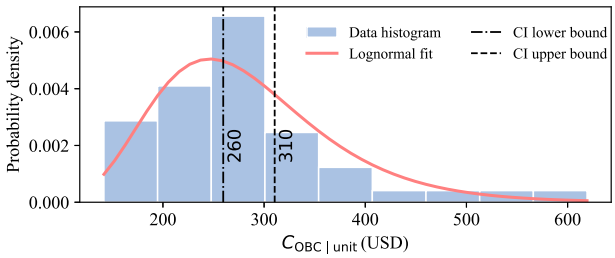

(a) Probability density of the cost of an IBB OBC unit considering around 36 discrete devices (data from [37]–[42]).

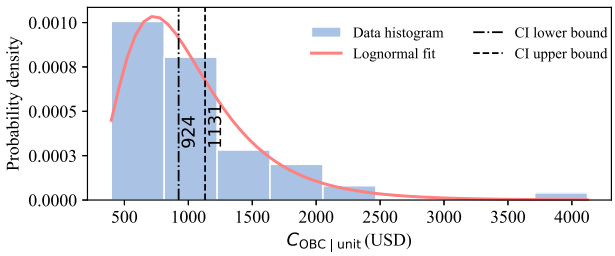

(b) Probability density of the cost of an IBB OBC unit considering around 60 devices, between half-bridge and full-bridge modules (data from [37]–[42]).

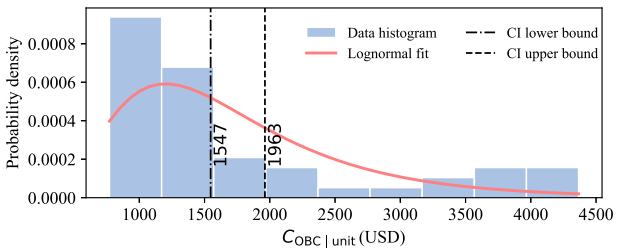

(c) Probability density of the cost of a DAB OBC unit considering around 48 devices, between half-bridge and full-bridge modules (data from [37]–[42]).

FIGURE 3. Probability density of the cost of 50 kW OBC units considering a lognormal distribution.

manufacturers: Infineon [37], Microchip [38], Onsemi [39], Rohm [40] Wolfspeed [41], and STMicroelectronics [42]. Both IBB and DAB topologies under evaluation require eight switches ($N_{\text{Sw|unit}} = 8$). Therefore, it is possible to estimate the cost of the switches for both converters, considering that it approximates a lognormal distribution. For the IBB, its cost based on discrete and module MOSFETs is illustrated in Fig. 3(a), and 3(b), respectively. The cost to compose a DAB converter based on module MOSFETs is shown in Fig. 3(c). A 90% confidence interval for the mean of the lognormal distribution is calculated, with a lower bound value of $C_{\text{Sw|lower}} = 260$ USD, and a upper bound value of $C_{\text{Sw|upper}} = 310$ USD considering discrete devices, and $C_{\text{Sw|lower}} = 924$ USD, $C_{\text{Sw|upper}} = 1131$ USD considering power modules for the IBB converter. More expensive

TABLE 2. $C_{\text{OBC|unit}}$ for the IBB and DAB Converter Unit Considering Sic MOSFET Modules

Converter	$C_{\text{Sw\|lower}}$	$C_{\text{Sw\|mean}}$	$C_{\text{Sw\|upper}}$
IBB	924.00 USD	1027.50 USD	1131.00 USD
DAB	1547.00 USD	1755.00 USD	1963.00 USD

values are estimated for the DAB converter due to the higher rated current, with a lower and upper bounds of $C_{\text{Sw|lower}} = 1547$ USD, and $C_{\text{Sw|upper}} = 1963$ USD. These values are summarized in Table 2, which also reports the mean cost ($C_{\text{Sw|mean}}$) of the SiC MOSFET modules required per converter unit of 50 kW.

It is also worth mentioning the cost of the gate drivers. Due to the similarities between the IBB and DAB converter already commented in Section I-B, the gate driver requirements are essentially the same for both solutions. The two converters rely on isolated gate drivers to ensure safe operation and compliance with insulation requirements in high-power applications that utilize SiC MOSFET devices and operate at the same switching frequencies. Therefore, both converters can use the same class of commercially available isolated gate driver and auxiliary isolated power supplies. Consequently, differences in gate driver implementation would not significantly affect the overall OBC cost, and do not represent a discriminating factor in the comparative assessment of the two converter topologies. Due to these factors, the cost of gate drivers was not considered.

C. OUTPUT FILTER AND CONDUCTOR SPECIFICATIONS

The IBB was designed to operate with a maximum output current ripple of 20%, which occurs when the converter operates as a boost (refer to (1)) with a duty-cycle equal to $D = 0.5$, corresponding to input and output voltages of $V_{\text{in}} = 380$ V and $V_{\text{out}} = 760$ V, respectively. The LC filter was then designed with a natural frequency ten times lower than the switching frequency to attenuate this ripple. As a result, the ripple of the current on the load side of the IBB after LC filter actuation becomes comparable to that of the DAB converter under the same filtering conditions. Regarding the output filter losses impact in the efficiency analysis, the small inductance value and the low equivalent series resistance of film capacitors suitable for this application [45] make the associated losses significantly smaller than those of the power-stage components. For this reason, and to simplify the analysis, the filter losses were omitted.

To mitigate skin effect, the conductors used in the magnetic components of the converters are implemented using multi-strand Litz wire. Following the guidelines in [26], AWG 30 is selected for the individual strands, corresponding to a strand radius of approximately 0.13 mm [46]. Since the strand radius is smaller than the skin depth for the considered operating frequencies, the current distribution within each strand remains nearly uniform, and skin effect can therefore be considered

TABLE 3. Magnetic Component Comparison for IBB and DAB Converter At Different Switching Frequencies

Frequency	Converter	Magnetic Component[1]	Core type[2]	Inductance	Weight	Volume	Core Count	Inductor/ HFT Count	Weight Ratio	Volume Ratio	Cost per unit
100 kHz	IBB	Inductor	UU 93/76/16	217 μH	800 g	0.159 dm^3	1	2			19.70 USD
	DAB	HFT	UU 126/91/20	6.03 μH	1300 g	0.269 dm^3	1	1	0.84	0.83	51.00 USD
	DAB	Inductor	UI 93/76/16	3.07 μH	600 g	0.116 dm^3	1	1			19.70 USD
75 kHz	IBB	Inductor	UU 93/76/20	290 μH	1000 g	0.198 dm^3	1	2			13.96 USD
	DAB	HFT	UU 126/91/20	8.05 μH	1300 g	0.269 dm^3	1	1	1.05	1.03	51.00 USD
	DAB	Inductor	UI 93/76/16	4.28 μH	600 g	0.116 dm^3	1	1			19.70 USD
50 kHz	IBB	Inductor	UU 93/76/30	436 μH	1500 g	0.297 dm^3	1	2			15.50 USD
	DAB	HFT	UU 126/91/20	12.00 μH	1300 g	0.269 dm^3	1	1	1.58	1.52	51.00 USD
	DAB	Inductor	UI 93/76/16	6.40 μH	600 g	0.116 dm^3	1	1			19.70 USD
25 kHz	IBB	Inductor	UU 93/76/30	872 μH	3000 g	0.594 dm^3	2	2			15.50 USD
	DAB	HFT	UU 126/91/20	24.00 μH	2600 g	0.538 dm^3	2	1	1.87	1.81	51.00 USD
	DAB	Inductor	UU 93/76/20	15.50 μH	600 g	0.116 dm^3	1	1			13.96 USD

[1] Material (N87) specifications for the components are provided in [43].
[2] Datasheets of TDK cores are provided in [44].

negligible at the strand level. Moreover, each strand is capable of carrying a maximum current of approximately 142 mA [46]. Based on these considerations, the converter current density is limited to $J = 5$ A/mm^2. In addition to skin effect, the proximity effect can also contribute to increasing copper losses. According to [47], this effect can be accounted for by introducing a resistance factor (F_r) that multiplies the DC resistance of the conductor. The resulting effective resistance is therefore given by $R_{res} = F_r R_{DC}$. Therefore, the manuscript adopts a conservative value of $F_r = 1.2$ to evaluate the copper losses.

D. MAGNETIC COMPONENTS SPECIFICATIONS

The specifications of the magnetic components adopted in the proposed IBB and DAB converters are presented, including the power transfer inductance and the HFT. The required DAB inductance to ensure the converter can deliver 50 kW across the entire input and output voltage range was calculated so that full power delivery is possible even under the lowest voltage conditions at both input and output, without exceeding the current limits of 87.5 V (input) and 77.5 V (output). This worst-case scenario occurs when the input voltage is 571 V, and the output voltage is 645 V. In this condition, the outer phase shift reaches its maximum value of $\phi_2 = 0.25$. The DAB inductance for power transfer is designed using an auxiliary inductor and a HFT with a theoretical leakage inductance referred to the primary side, calculated according to the guidelines in (8). The design of the HFT to achieve the target leakage inductance depends on constructive parameters already described in Section II-B. In this work, the maximum value for I_m is specified as a fraction of the maximum current flowing through the HFT, which occurs at the rated converter power of 50 kW with $V_{in} = 571$ V and $V_{out} = 645$ V. Under these conditions, the maximum input and output currents in the converter are 87.5 A and 77.5 A (Table 1), respectively. However, time-domain simulations show that the RMS current in the HFT windings is significantly higher than the converter's input current, reaching approximately 136 A. To ensure a conservative design, the windings were dimensioned for a current of 136 A and further increased by considering a utilization factor of 85%, resulting in a final current capability of 160 A. In this work, the HFTs were designed such that the I_m reaches a maximum value of 7% of the maximum HFT operating current. The coupling coefficient is assumed to be $k_c = 0.98$, which is more conservative than values reported in the literature [48], [49]. The window utilization factor (K_u), which is calculated based on transformer window area (A_w), is considered to be up to 30% for all magnetic devices, based on guidelines from [50], [51].

The chosen magnetic cores used in the considered converters are made of Siferrit material N87, whose properties are detailed in [43]. Considering the mentioned converters' design parameters, Table 3 displays the core specifications of the magnetic components for both converters, including the core type, weight, volume, and cost evaluated based on the search engine [52]. The design considers the switching frequencies of 100 kHz, 75 kHz, 50 kHz, and 25 kHz. One can observe that the weight of magnetic components is reduced when f_{Sw} grows, as predicted. However, the weight of magnetic components needed by the IBB converter concerning the DAB significantly decreases from 1.87 at 25 kHz to 0.84 at 100 kHz. The same can be observed for its volume, whose ratio drops from 1.81 to 0.83 for the mentioned frequencies. This suggests that the IBB converter benefits more from higher switching frequencies in terms of magnetic size reduction than DAB converters. There is also a crossover near 75 kHz, where the ratio is around 1.05 and 1.03 for weight and volume, respectively, indicating that both converters require magnetic components with similar weight and volume. For frequencies below 75 kHz, the DAB maintains an advantage in magnetic compactness. The Core Count column in Table 3 indicates the number of cores required to achieve

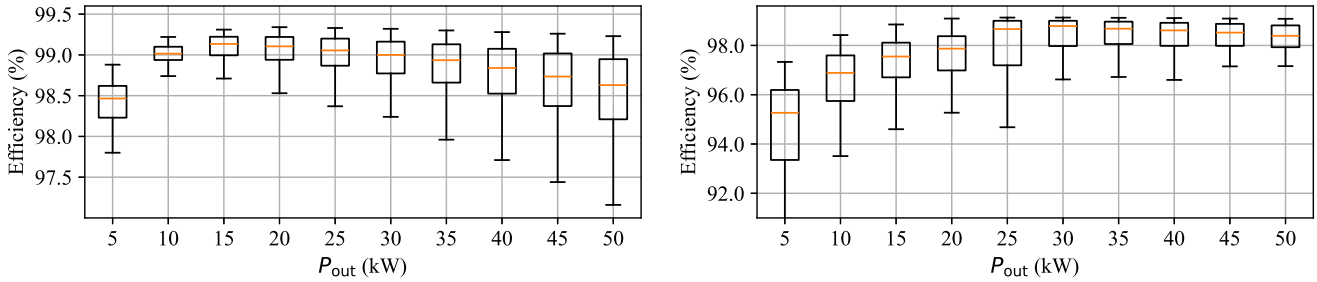

(a) Boxplots representing the IBB converter efficiencies.

(b) Boxplots representing the DAB converter efficiencies.

FIGURE 4. Boxplots representing the converter's efficiencies at $f_{sw} = 75$ kHz for different catenary, battery, and P_{out} levels. The DPS modulation is used for the DAB converter up to the power level of $P_{out} = 20$ kW.

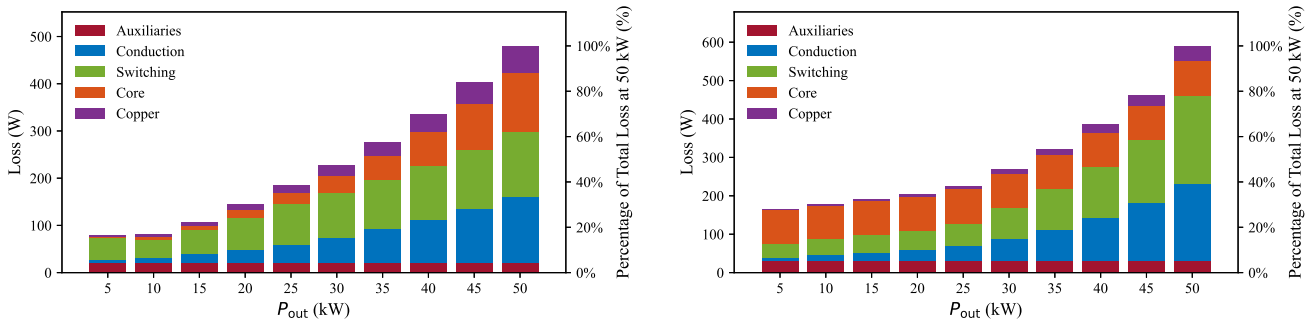

(a) Losses breakdown for the IBB considering $V_{in} = 690\,V$ and $V_{out} = 675\,V$.

(b) Losses breakdown for the DAB considering $V_{in} = 690\,V$ and $V_{out} = 675\,V$.

FIGURE 5. Losses breakdown for the IBB and DAB converter for $f_{sw} = 75$ kHz in function of the output power.

TABLE 4. HFT Specifications to Reach Target Leakage Inductance

Frequency	Core type	N_1	K_u	A_c	l_c	l_g	A_w
100 kHz	UU 126/91/20	41	30%	560 mm^2	480 mm	3.8 mm	8820 mm^2
75 kHz	UU 126/91/20	34	24%	560 mm^2	480 mm	1.9 mm	8820 mm^2
50 kHz	UU 126/91/20	36	26%	560 mm^2	480 mm	1.4 mm	8820 mm^2

the desired inductance for the application. Specifically for 25 kHz frequency, two cores are required in parallel, which can be more challenging to implement in practice. Therefore, for simplification purposes, the following analyses consider converters operating at frequencies of 100 kHz, 75 kHz, and 50 kHz. Finally, Table 4 specifies the values for the HFT parameters to reach the target leakage inductance exhibited in Table 3.

The losses in the magnetic core are evaluated based on the Steinmetz equation, whose parameters were extracted from the datasheet information provided for the N87 core material [43]. The datasheet provides the core losses in $\frac{kW}{m^3}$ as a function of frequency, for magnetic flux densities of 50 mT, 100 mT, and 200 mT, at the temperatures of 25 °C and 100 °C. The magnetic components (inductors and high-frequency transformers) used in both converters were designed to operate with a maximum flux density of 300 mT, consistent with datasheet recommendations. For each flux level, the corresponding datasheet curve was interpolated, and the Steinmetz coefficients were extracted. The average power loss per unit volume can be estimated based on the equation:

$$P_v = k f_{Sw}^{\alpha} B^{\beta}, \tag{17}$$

where B is the peak magnetic flux density, k, α, and β are the Steinmetz coefficients. Based on the extracted parameters, the simulation model computes the core losses at each simulation step. The variable B is calculated by (6), and (12), and the Steinmetz parameters used in this work are: $k = 74.6$, $\alpha = 1.3$, $\beta = 2.8$. Using these parameters, the normalized root-mean-square error (NRMSE) between the datasheet core-loss curves and the model predictions is 4.2% at 50 mT, 5.8% at 100 mT, and 6.1% at 200 mT, indicating agreement between the datasheet information and the core-loss calculation model used in the simulation.

V. RESULT ANALYSIS

This section provides the simulation results evaluating the efficiency of the studied converter topologies under different switching frequencies, various input and output voltages, and output power levels. Initially, the theoretical efficiency characterization of the 50 kW converter module for both topologies

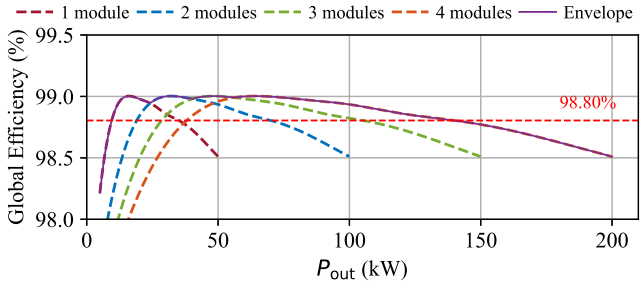

(a) Efficiency curves for IBB converter at $f_{Sw} = 100\,\text{kHz}$.

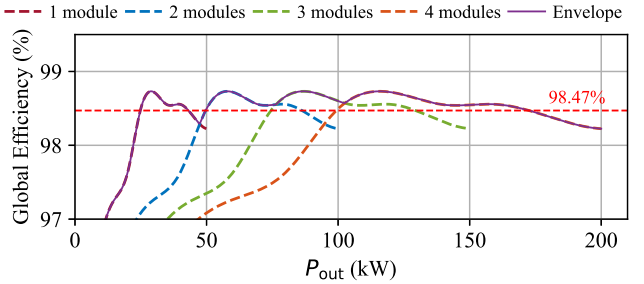

(b) Efficiency curves for DAB converter at $f_{Sw} = 100\,\text{kHz}$.

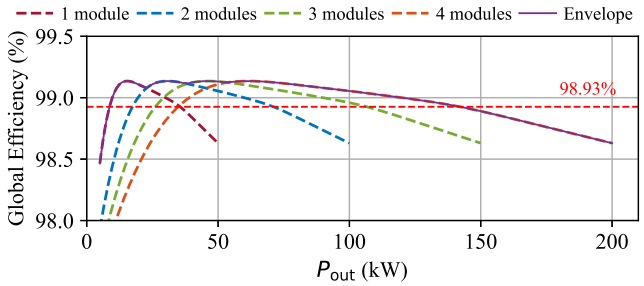

(c) Efficiency curves for IBB converter at $f_{Sw} = 75\,\text{kHz}$.

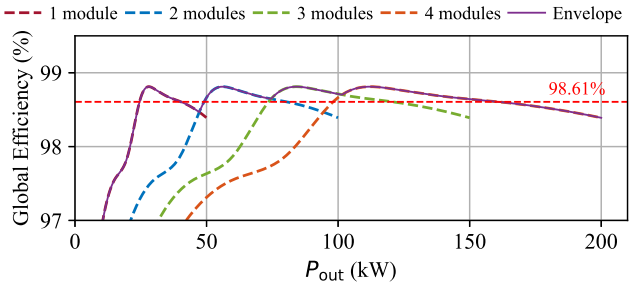

(d) Efficiency curves for DAB converter at $f_{Sw} = 75\,\text{kHz}$.

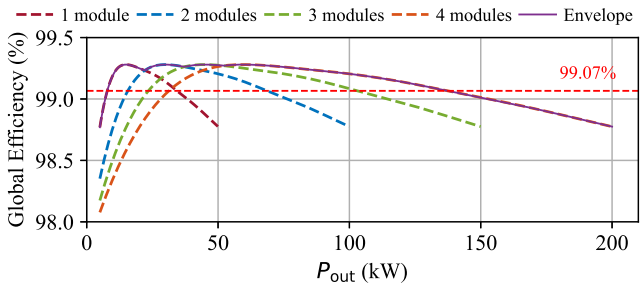

(e) Efficiency curves for IBB converter at $f_{Sw} = 50\,\text{kHz}$.

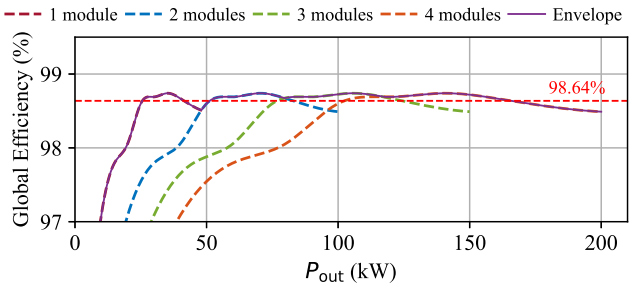

(f) Efficiency curves for DAB converter at $f_{Sw} = 50\,\text{kHz}$.

FIGURE 6. Efficiency curves for the converters considering module shedding. The DPS modulation is used for the DAB converter up to the power level of $P_{out} = 20$ kW. The red dashed lines represent the four-point efficiency.

will be presented under various operating conditions, with input and output voltages and converter output power being varied. Next, the efficiency characterization of the four modules in operation will be presented to achieve the 200 kW power required for the application.

The boxplots exhibited in Fig. 4(a) and 4(b), shows respectively, the IBB and DAB converters' efficiency distribution as a result of a sweep simulation on input and output voltage from their minimum to maximum values at different output power (P_{out}) levels, that vary from 5 kW to 50 kW. For the DAB converter, DPS modulation is used for power levels up to 20 kW, while SPS modulation is applied for higher power levels, as can be observed in the discontinuity of DAB efficiency at 25 kW. The chosen switching frequency is 75 kHz, because the magnetic components for both converters have similar weight and volume values. Therefore, the efficiency of the two converters can be characterized for a relatively similar volume and weight. The line inside the box represents the median (50th percentile). The bottom and top edges of the box correspond to the 25th percentile and 75th percentile, respectively. The whiskers represent the maximum and minimum values. One can conclude from this efficiency characterization that, although the IBB efficiency is higher that of the DAB at most of operating points due to efficiency levels above 99%, the DAB converter exhibits a high-efficiency plateau, with the median efficiency stabilizing at values higher than 98% for output powers above 25 kW.

To complete the analysis of the power-converter modules, Fig. 5 presents the loss breakdown of the IBB and DAB converters as a function of output power, considering semiconductor switching and conduction losses, as well as magnetic core and copper losses. The analysis is performed for an operating condition with $V_{in} = 690$ V, and $V_{out} = 675$ V, which correspond to the average values within the input and output voltage ranges of the converters. At the rated power of 50 kW, the IBB converter exhibits the following loss distribution: conduction and switching losses each represent about 29%, while core, copper, and auxiliary losses

TABLE 5. Efficiency Assessment for the IBB and DAB Converters

Frequency	Load point	IBB Efficiency	DAB Efficiency	ΔEfficiency
100 kHz	η_{100}	98.50%	98.22%	0.28 pp
	η_{75}	98.77%	98.55%	0.22 pp
	η_{50}	98.93%	98.59%	0.34 pp
	η_{25}	99.00%	98.52%	0.48 pp
	η_{4pt}	**98.80%**	**98.47%**	**0.33 pp**
75 kHz	η_{100}	98.63%	98.39%	0.24 pp
	η_{75}	98.89%	98.64%	0.25 pp
	η_{50}	99.05%	98.71%	0.34 pp
	η_{25}	99.13%	98.68%	0.45 pp
	η_{4pt}	**98.93%**	**98.61%**	**0.32 pp**
50 kHz	η_{100}	98.78%	98.49%	0.29 pp
	η_{75}	99.01%	98.72%	0.29 pp
	η_{50}	99.20%	98.73%	0.47 pp
	η_{25}	99.27%	98.61%	0.66 pp
	η_{4pt}	**99.07%**	**98.64%**	**0.43 pp**

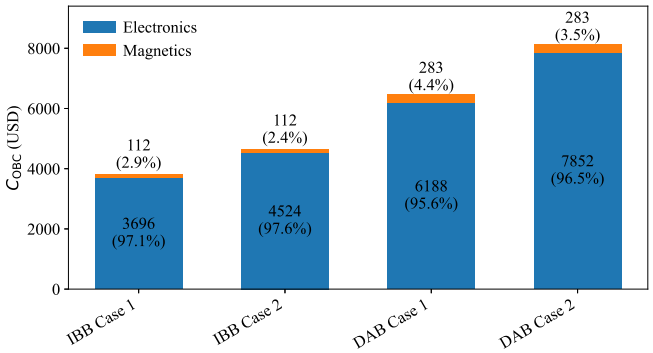

FIGURE 7. 200 kW OBC costs composed by modules of IBB and DAB converters. IBB Case 1 and DAB Case 1 are calculated based on $C_{Sw|lower}$, and IBB Case 2 and DAB Case 2 are calculated based on $C_{Sw|upper}$.

correspond to 26%, 12%, and 4%, respectively. For the DAB converter, conduction losses account for approximately 34%, switching losses for 39%, core losses for 16%, copper losses for 6%, and auxiliary losses for 5%.

For switching frequencies of 100 kHz, 75 kHz, and 50 kHz, Fig. 6 show the efficiencies of the converters under analysis, considering parallel operation controlled by the module shedding technique [29], [30], [31]. Although the theoretical efficiency of the DAB converter is relatively lower than that of the IBB, as shown in Fig. 4, the converters' average efficiencies – based on a four-point evaluation at 25%, 50%, 75%, and 100% of the maximum power (200 kW) – operating with module-shedding techniques present similar values, as exhibited in Table 5. A slight advantage for the IBB converter can be observed, with a difference in percentage points (pp) of approximately 0.33 pp, 0.32 pp, and 0.43 pp (Table 5) for the respective switching frequencies.

Considering the $C_{OBC|unit}$ for both the IBB and DAB converter units exhibited in Fig. 3, and the magnetic component costs listed in Table 3 it is possible to estimate the total cost for both 200 kW IBB and DAB converters, based on the 90% confidence interval for the mean of the lognormal distribution, and referring to (16) where $P_{inst} = 200$ kW, and $P_{inst|unit} = 50$ kW. For the IBB one, the total cost ranges from 3808 USD to 4636 USD, while for the DAB converter, it ranges from 6471 USD to 8135 USD, representing an increase of approximately 70% to 75%. The cost of the magnetic devices in comparison to the MOSFET modules' costs is compared in Fig. 7, and it represents just a small part in comparison to the electronics devices ones, quantified at a maximum of 4.4% of the costs, referring to the case indicated as DAB Case 1.

The analysis performed in this work enables the proposal of a decision-making process for selecting the most suitable OBC topology for IMC buses. According to the applicable standards, second-level isolation is mandatory for this type of application. Therefore, manufacturers have two equivalent options to meet this requirement: providing mechanical isolation or adopting an isolated converter topology (Fig. 1). While both approaches satisfy the isolation requirement, they

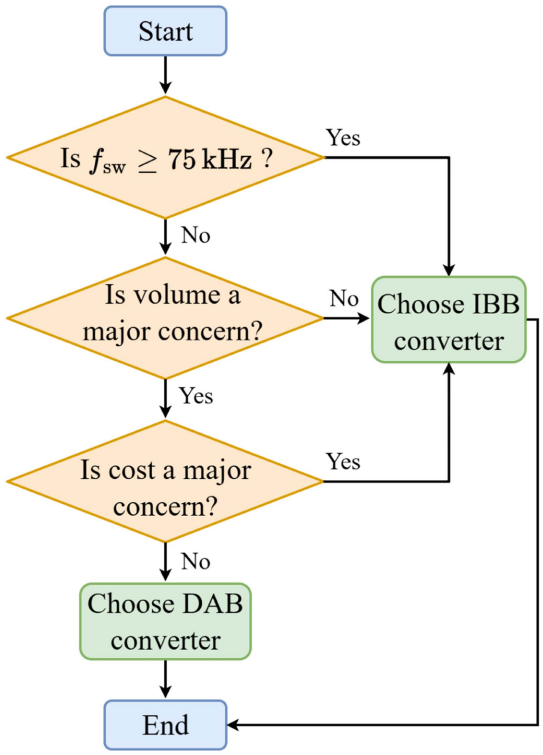

FIGURE 8. Flowchart representing the decision-making process for selecting the appropriate OBC topology.

lead to different design implications for the magnetic components, as well as different outcomes in terms of efficiency, volume, and cost. These trade-offs also depend on the chosen switching frequency. The decision-making process can be summarized in the flowchart of Fig. 8, where the IBB converter is clearly the chosen topology for f_{Sw} higher or equal than 75 kHz. If the chosen switching frequency is lower than the mentioned value, the volume, weight, and cost become the major decision-making criteria. In case volume is not a major concern for the manufacturer, the IBB topology is still recommended. However, in cases of substantial concerns regarding

volume and weight, the DAB topology is recommended if the converter's higher cost is not a key issue for the company.

VI. CONCLUSION

Driven by the need for high-efficiency, compact, and cost-reducing technologies in electrified public transportation, this work compares a non-isolated interleaved buck-boost (IBB) converter with an isolated dual-active-bridge (DAB) topology acting as an on-board-charger (OBC) for in-motion-charging (IMC) trolleybuses in terms of efficiency, weight, volume, and cost. From the results, both converters achieve similar efficiency levels considering 4 modules of 50 kW operating in coordination at switching frequencies of 100 kHz, 75 kHz, and 50 kHz. A slight advantage was observed for the IBB, which reaches average efficiency improvements in comparison to the DAB of around 0.33 pp, 0.32 pp, and 0.43 pp, for the mentioned switching frequencies. In terms of magnetic components, IBB emerges as the best choice for switching frequencies higher or equal than 75 kHz due to significant compactness in magnetic components in comparison to the DAB converter, while for frequencies lower than 75 kHz, the isolated alternative becomes competitive, due to its magnetic size advantage. When the costs of converters are discussed, the DAB converter presents costs higher than the IBB by approximately 70% to 75%, based on a 90% confidence level for the mean of the lognormal distribution characterizing the cost of automotive-grade MOSFETS modules. Therefore, the use of IBB topology is suggested if the design goal is high-frequency operation, and the DAB topology is suggested if operation is intended mainly at lower frequencies, where its disadvantages diminish. These results provide guidelines for selecting the optimal OBC topology depending on the intended switching frequency, benefiting both professionals from academic and industrial sectors. Future work can go in the direction of comparing the considered topologies in terms of safety, as well as investigating the influence of battery technologies and charging techniques in the decision-making process for selecting the appropriate OBC topology.

REFERENCES

[1] European Commission, "The European green deal" Communication from the commission to the European Parliament, Brussels, 2019. Accessed: Sep. 09, 2025. [Online]. Available: https://eur-lex.europa.eu

[2] European Commission and Directorate-General for Climate Action, "Going climate-neutral by 2050: A strategic long-term vision for a prosperous, modern, competitive and climate-neutral EU economy," publications Office of the European Union, Luxembourg, 2019. Accessed: Sep. 09, 2025. [Online]. Available: https://op.europa.eu

[3] Governo do Brasil, "Programa de mobilidade verde," 2025. Accessed: Sep. 09, 2025. [Online]. Available: https://www.gov.br/planalto/pt-br/acompanhe-o-planalto/noticias/2023/12/mover-novo-programa-amplia-acoes-para-mobilidade-verde-e-descarb

[4] Via Trolebus, "Trolleybus in the city of São Paulo," Accessed: Sep. 09, 2025. [Online]. Available: https://viatrolebus.com.br/2013/03/haddad-fala-sobre-sistema-trolebus-em-sao-paulo/

[5] M. Bartłomiejczyk, "Practical application of in motion charging: Trolleybuses service on bus lines," in *Proc. Int. Sci. Conf. Electr. Power Eng.*, 2017, pp. 1–6.

[6] F. Bergk, K. Biemann, U. Lambrecht, D. Prof, and R. Pütz, "Potential of in-motion charging buses for the electrification of urban bus lines," *J. Earth Sci. Geotech. Eng.*, vol. 6, no. 4, pp. 347–362, 2016.

[7] R. F. P. Paternost, I. Diab, G. R. C. Mouli, M. Ricco, P. Bauer, and G. Grandi, "Stationary energy storage solutions and power management for bus fleet electrification in congested grid areas," *IEEE Access*, vol. 12, pp. 140211–140222, 2024.

[8] I. Diab, R. Eggermont, G. R. Chandra Mouli, and P. Bauer, "An adaptive battery charging method for the electrification of diesel or CNG buses as in-motion-charging trolleybuses," *IEEE Trans. Transport. Electrific.*, vol. 9, no. 3, pp. 4531–4540, Sep. 2023.

[9] D. Bündgen, N. Fritz, A. Thönnessen, T. Kamp, and R. W. D. Doncker, "Powering next-generation catenary trucks—A compact, bidirectional 200 kW on-board charger," *IEEE Trans. Transport. Electrific.*, vol. 10, no. 4, pp. 8050–8061, Dec. 2024.

[10] *Electrically Propelled Road Vehicles — Safety Specifications*, Standard ISO 64693:2021, The British Standards Institution, Geneva, Switzerland, 2021.

[11] *Protection Against Electric Shock — Common Aspects for Installation and Equipment*, Stadnard EN 61140:2016, CENELEC, Brussels, Belgium, 2016.

[12] *Electric Vehicle Conductive Charging System*, Standard EN 61851-23:2014, CENELEC, Brussels Belgium, 2014.

[13] L. Shams Ashkezari, H. J. Kaleybar, and M. Brenna, "Electric bus charging infrastructures: Technologies, standards, and configurations," *IEEE Access*, vol. 12, pp. 80505–80528, 2024.

[14] M. Yilmaz and P. T. Krein, "Review of battery charger topologies, charging power levels, and infrastructure for plug-in electric and hybrid vehicles," *IEEE Trans. Power Electron.*, vol. 28, no. 5, pp. 2151–2169, May 2013.

[15] M. ElMenshawy and A. Massoud, "Medium-voltage DC-DC converter topologies for electric bus fast charging stations: State-of-the-art review," *Energies*, vol. 15, no. 15, 2022, Art. no. 5487.

[16] R. F. P. Paternost, M. V. De Paula, R. Mandrioli, M. Ricco, and T. A. Dos Santos Barros, "Comparative analysis of isolated and non-isolated on-board-charger topologies for electric buses," in *Proc. Brazil. Power Electron. Conf.*, 2025, pp. 1–6.

[17] X. Zhu, "A dual-active-bridge converter for novel trolleybus powertrain system," in *Proc. Asian Conf. Energy, Power Transp. Electrific.*, 2018, pp. 1–6.

[18] N. Fritz, D. Bündgen, I. Austrup, and R. W. De Doncker, "A simple, decoupled control concept for a modular DC-DC converter in isop, ipop, and back-to-back connection," in *Proc. IEEE Workshop Control Model. Power Electron.* 2021, pp. 1–8.

[19] D. Bündgen, A. Thönnessen, N. Fritz, T. Kamp, and R. W. De Doncker, "Highly integrated 200 KW SiC three-phase dual-active-bridge converter with 3D-printed fluid coolers," in *Proc. IEEE Workshop Wide Bandgap Power Devices Appl.*, 2021, pp. 182–187.

[20] A. V. Stoian, J. Geng, S. Baldisserri, F. M. Tiburtini, M. Ricco, and R. Mandrioli, "Performance evaluation of DAB-based partial power processing for in-motion-charging trolleybuses," in *Proc. IEEE Int. Conf. Compat., Power Electron. Power Eng.*, 2025, pp. 1–6.

[21] M. Lukianov, E. Romero-Cadaval, A. Kasprowicz, O. Husev, and R. Strzelecki, "Scalable multiport DC-DC converter for bidirectional EV charging in DC traction grids," *IEEE Trans. Circuits Syst. II, Exp. Briefs*, vol. 72, no. 7, pp. 968–972, Jul. 2025.

[22] *Railway Applications—Supply Voltages of Traction Systems*, Standard EN 50163:2004+A2:2020, CENELEC, Brussels, Belgium, 2020.

[23] R. F. Paternost, R. Mandrioli, V. Cirimele, M. Ricco, and G. Grandi, "Solutions for retrofitting catenary-powered transportation systems toward greater electrification in smart cities," *Smart Cities*, vol. 7, no. 6, pp. 3853–3870, 2024.

[24] Kiepe Electric, "IMC500/E-BUS with in-motion-charging (IMC)," Accessed: Jun. 23, 2025. [Online]. Available: https://kiepe.knorr-bremse.com/en/de/buses-and-e-mobilty/e-systems/imc500-e-bus-with-in-motion-charging-imc/

[25] M. Beraki, J. P. Trovão, and M. Perdigao, "Design of variable inductor for powertrain DC-DC converter," in *Proc. IEEE Int. Symp. Ind. Electron.*, 2019, pp. 822–827.

[26] S. Dey, S. S. Chakraborty, S. Singh, and K. Hatua, "Design of high frequency transformer for a dual active bridge (DAB) converter," in *Proc. IEEE Glob. Conf. Comput. Power Commun. Technol.*, 2022, pp. 1–6.

[27] M. Turzyński et al., "Analytical estimation of power losses in a dual active bridge converter controlled with a single-phase shift switching scheme," *Energies*, vol. 15, no. 21, 2022, Art. no. 8262.

[28] B. Zhao, Q. Song, and W. Liu, "Power characterization of isolated bidirectional dual-active-bridge DC–DC converter with dual-phase-shift control," *IEEE Trans. Power Electron.*, vol. 27, no. 9, pp. 4172–4176, Sep. 2012.
[29] J. W. Kolar, F. Krismer, Y. Lobsiger, J. Muhlethaler, T. Nussbaumer, and J. Minibock, "Extreme efficiency power electronics," in *Proc. Int. Conf. Integr. Power Electron. Syst.*, 2012, pp. 1–22.
[30] J.-T. Su and C.-W. Liu, "A novel phase-shedding control scheme for improved light load efficiency of multiphase interleaved DC–DC converters," *IEEE Trans. Power Electron.*, vol. 28, no. 10, pp. 4742–4752, Oct. 2013.
[31] J. Geng et al., "Performance evaluation of DAB-based partial- and full-power processing for BESS in support of trolleybus traction grids," *Electronics*, vol. 14, no. 14, 2025, Art. no. 2871.
[32] P. Camail, B. Allard, M. Darnon, C. Joubert, C. Martin, and J. P. F. Trovão, "Overview of DC/DC converters for concentrating photovoltaics (CPVs)," *Energies*, vol. 16, no. 20, 2023, Art. no. 7162.
[33] Kiepe Electric, "Kiepe insulating converter KIC 200, 300," Accessed: Jun. 23, 2025. [Online]. Available: https://kiepe-group.com/produkte/bus/bordnetzenergieversorgung/kiepe-isolierender-converter-kic-200-300
[34] STMicroelectronics, "Automotive-grade SiC power MOSFET," Accessed: Jun. 23, 2025. [Online]. Available: https://www.st.com/en/power-transistors/sct015w120g3-4ag.html
[35] Wolfspeed, "Silicon carbide, half-bridge module," Accessed: Jun. 23, 2025. [Online]. Available: https://www.wolfspeed.com/products/power/sic-power-modules/wolfspeed-wolfpack-sic-power-modules-family/cab004m12gm4/
[36] Plexim, "PLECS—The standard simulation software for power electronics," Accessed: Jun. 23, 2025. [Online]. Available: https://www.plexim.com/products/plecs
[37] Infineon Technologies, "MOSFET modules (Si/SiC)," Accessed: Jun. 23, 2025. [Online]. Available: https://www.infineon.com/cms/en/product/power/mosfet/modules
[38] Microchip Technology, "Silicon carbide (SiC) modules for power electronics," Accessed: Jun. 23, 2025. [Online]. Available: https://www.microchip.com/en-us/products/power-management/silicon-carbide-sic-devices-and-power-modules/sic-modules
[39] Onsemi, "Silicon carbide (SiC) modules," Accessed: Jun. 23, 2025. [Online]. Available: https://www.onsemi.com/products/discrete-power-modules/power-modules/silicon-carbide-sic-modules
[40] ROHM Semiconductor, "SiC power module," Accessed: Jun. 23, 2025. [Online]. Available: https://www.rohm.com/products/sic-power-devices/sic-power-module
[41] Wolfspeed, "Silicon carbide power modules," Accessed: Jun. 23, 2025. [Online]. Available: https://www.wolfspeed.com/products/power/sic-power-modules/
[42] STmicroelectronics, "SiC MOSFETs," Accessed: Jun. 23, 2025. [Online]. Available: https://www.st.com/en/sic-devices/sic-mosfets.html
[43] TDK Electronics, "Ferrites and accessories - SIFERRIT material N87," Accessed: May 28, 2025. [Online]. Available: https://www.tdk-electronics.tdk.com/download/528882/990c299b916e9f3eb7e44ad563b7f0b9/pdf-n87.pdf
[44] TDK Electronics, "Large-size ferrite cores," Accessed: May 28, 2025. [Online]. Available: https://www.tdk-electronics.tdk.com/en/3261404/products/product-catalog/ferrites-and-accessories/large-size-cores
[45] TDK Electronics, "Film capacitors–power electronic capacitors," Accessed: May 28, 2025. [Online]. Available: https://www.tdk-electronics.tdk.com/download/528882/990c299b916e9f3eb7e44ad563b7f0b9/pdf-n87.pdf
[46] PowerStream, "Wire gauge and current limits including skin depth and tensile strength," Accessed: Apr. 08, 2025. [Online]. Available: https://www.powerstream.com/Wire_Size.htm
[47] C. R. Sullivan, "Optimal choice for number of strands in a litz-wire transformer winding," *IEEE Trans. Power Electron.*, vol. 14, no. 2, pp. 283–291, Mar. 1999.
[48] T. O. Howard and K. H. Carpenter, "A numerical study of the coupling coefficients for pot core transformers," *IEEE Trans. Magn.*, vol. 31, no. 3, pp. 2249–2253, May 1995.
[49] S. Lee, H. Cha, and D.-C. Lee, "Voltage balancing for triple-active-bridge converter using integrated transformer," *IEEE J. Emerg. Sel. Topics Power Electron.*, vol. 13, no. 2, pp. 2027–2035, Apr. 2025.
[50] J. W. McLean, "Inductor design using amorphous metal C-cores," *IEEE Circuits Devices Mag.*, vol. 12, no. 5, pp. 26–30, Sep. 1996.
[51] M. A. Moonem, C. L. Pechacek, R. Hernandez, and H. Krishnaswami, "Analysis of a multilevel dual active bridge (ML-DAB) DC-DC converter using symmetric modulation," *Electronics*, vol. 4, no. 2, pp. 239–260, 2015.
[52] Octopart, "The electronic part search engine," Accessed: Apr. 08, 2025. [Online]. Available: https://octopart.com/

RUDOLF F. P. PATERNOST (Member, IEEE) received the bachelor's degree in electrical engineering from the University of São Paulo, São Paulo, Brazil, in 2017, the master's degree in electrical engineering from the State University of Campinas (UNICAMP), Campinas, Brazil, in 2019, and the Ph.D. degree in automotive engineering for intelligent mobility from the University of Bologna, Bologna, Italy, in 2024. He was involved in teaching activities for engineering courses and was a Visiting Ph.D. Candidate with the Faculty of Electrical Engineering, Delft University of Technology, Delft, The Netherlands. He is currently a Postdoctoral Researcher with the Faculty of Electrical and Computer Engineering, UNICAMP. His doctoral research focused on proposing solutions to modernize the electrical infrastructure of catenary-powered transportation systems, enabling the integration of emerging technologies, such as in-motion charging vehicles and energy storage systems. His research focuses on power electronics converters for electric bus charging.

RICCARDO MANDRIOLI (Senior Member, IEEE) received the Ph.D. (Hons.) degree in biomedical, electrical, and system engineering from the University of Bologna, Bologna, Italy, in 2023. From 2022 to 2024, he has been a Postdoctoral Research Fellow and Adjunct Professor, and he has also been involved as a Teaching Assistant for multiple engineering courses since 2017. In 2022, he was a Visiting Scientist with the Chair of Power Electronics, Kiel University, Kiel, Germany. In 2023, he received the National Scientific Habilitation (ASN) for the permanent position of Associate Professor in electrical engineering. He is currently a Tenure Track Assistant Professor (RTT) of electrical engineering with the Department of Electrical, Electronic, and Information Engineering, University of Bologna. His research interests include electric vehicle chargers, photovoltaic, power electronic converters, harmonic pollution, efficiency improvement, and circuit modeling. Dr. Mandrioli was the winner of several awards with IEEE. He is an Associate Editor for IEEE ACCESS and Editorial Board Member of several journals.

IBRAHIM DIAB (Member, IEEE) received the bachelor's degree in mechanical engineering from the American University of Beirut, Beirut, Lebanon, in 2012, and the Ph.D. degree from DCE&S Group, Electrical Engineering Faculty, Delft University of Technology (TU Delft), Delft, The Netherlands, on transforming the trolleybus grid into an active, sustainable, and multifunctional electrical infrastructure. In 2015, he received the TU Delft "Delft Research Initiative-Energy" Full Scholarship and joined the Sustainable Energy Technologies master's program of the Electrical Engineering Faculty (2017, honors). From 2022 to 2024, he was a Postdoctoral Research Fellow jointly with the AMS Institute, Amsterdam, and the DCE&S Group, TU Delft, on integrating electric bus chargers in the metro grid of the public transport operator of Amsterdam, the GVB, with whom he has been working since.

Since 2024, he has been an Independent Consultant working on a number of Dutch and European projects, such as multi-functional traction grids, fleet electrification, EV charging infrastructures, circularity in transport grids, and DC energy hubs.

MIKOLAJ BARTŁOMIEJCZYK (Member, IEEE) received the Ph.D. degree in electrical engineering and a habilitation focused on reducing energy consumption in zero-emission public transport systems. He was an Expert for organizations such as the EBRD and collaborates widely with European Research Centers. He has completed multiple international research placements at leading academic institutions, including Berner Fachhochschule (Biel, Switzerland), TU Delft (Netherlands), VŠB–TU Ostrava (Czech Republic), University of Žilina (Slovakia) and the Transport University in Rostov on Don (Russia), contributing to long-term collaborations in electromobility, energy storage and smart transport systems. He is currently an Associate Professor with the Gdańsk University of Technology, Gdańsk, Poland and an Energy Specialist with PKT Gdynia, where he is responsible for strategic development projects in the trolleybus power system and the integration of innovative technologies into public transport infrastructure. Mikołaj is the author of more than 100 scientific publications on electric bus charging strategies, traction power systems, and battery degradation modelling. His research interests include energy efficiency, dynamic in-motion-charging, second-life battery applications, and the role of trolleybus networks as urban smart grid platforms. He has led or co-led numerous international projects funded by Horizon Europe, Interreg and ERA NET, including Automat, EfficienCE, CE4CE, and Trolley 2.0.

MATTIA RICCO (Senior Member, IEEE) received the master's (*cum laude*) degree in electronic engineering from the University of Salerno, Fisciano, Italy, in 2011, and the Ph.D. double degree in electrical and electronic engineering from the University of Cergy-Pontoise, Cergy-Pontoise, France, and in information engineering from the University of Salerno in 2015. From 2015 to 2018, he was a Postdoctoral Research Fellow with the Department of Energy Technology, Aalborg University, Aalborg, Denmark. From 2018 to 2021, he was a Senior Assistant Professor (Tenure Track) and since 2021, he has been an Associate Professor with the Department of Electrical, Electronic, and Information Engineering, Alma Mater Studiorum - University of Bologna, Bologna, Italy. He is currently the Coordinator of the Power Electronic Circuits and Photovoltaic Research Group. His research interests include transportation electrification, electric vehicle chargers, modular multilevel converters, battery management system, field-programmable gate array-based controllers, reliability and circularity for power electronics, and photovoltaic systems. Dr. Ricco is the Editor of *IET Power Electronics* and Associate Editor for the IEEE TRANSACTIONS ON INDUSTRIAL ELECTRONICS. Since 2026, he has been the Vice-Chair of the IEEE Industrial Electronics Society – Italy Section Chapter.

TÁRCIO A. S. BARROS (Member, IEEE) received the technical degree in industrial electronics from SENAI-PE in 2004, the bachelor's (Hons.) degree in electrical engineering from the Federal University of the São Francisco Valley, Petrolina, Brazil, in 2010, and the M.Sc., Ph.D., and Habilitation (Livre Docência) degrees in electrical engineering from the University of Campinas (UNICAMP), Campinas, Brazil, in 2012, 2015, and 2022, respectively. He is currently an Associate Professor (MS5.1) with the School of Electrical and Computer Engineering (FEEC), UNICAMP. He is also a Member of the graduate faculties with the School of Mechanical Engineering (FEM) and FEEC-UNICAMP. He is the Coordinator of UNICAMP Electric Mobility Center (currently under development). His expertise lies in electrical engineering, with a focus on power electronics and electric machine drives for electric vehicles. His research interests include renewable energy generation (wind and solar), industrial electronics, electronic control systems, electromechanical device modeling, electronic instrumentation, and industrial automation. He is the Technical Coordinator for National Rota 2030 Program (Line V), focusing on biofuels, alternative propulsion, and vehicle safety. He is a member of the IEEE (Institute of Electrical and Electronics Engineers), SBA (Brazilian Society of Automatics), and SOBRAEP (Brazilian Power Electronics Society).

Coordenação de Aperfeiçoamento de Pessoal de Nível Superior (CAPES) - ROR identifier: 00x0ma614